Optica Applicata, Vol. XL, No. 1, 2010

Real-time mask-division technique based on DMD digital lithography

NINGNING LUO[1, 2*], YIQING GAO[2], MIN CHEN[2], LIXIA YU[2], QING YE[2]

[1]College of Automation Engineering, Nanjing University of Aeronautics and Astronautics, Nanjing 210016, P.R. China

[2]Key Laboratory of Nondestructive Test (Chinese Ministry of Education), Nanchang HangKong University, Nanchang 330063, P.R. China

[*]Corresponding author: ningningluo2002@yahoo.com.cn

Digital lithography technique is a promising tool for the fabrication of binary optical element. In this paper, we present the mask-division technique to improve the lithography quality. A piece of high-frequency mask is divided into several pieces of low-frequency binary masks. Then they are imaged on the photoresist successively by using the DMD-based lithography system. Based on the theory of partial coherent light, the intensity distribution in image plane has been simulated. The grating masks with period of 4 μm have been fabricated by using the mask-division technique. Experimental results demonstrate the feasibility of the proposed method as an effective technique for advancing the edge sharpness.

Keywords: digital lithography technique, mask-division technique, DMD-based lithography, edge sharpness.

1. Introduction

In recent years, a digital lithography technique employing a spatial light modulator (SLM) as a pattern generator has caught wide attention. Many papers report the application of DMD for digital lithography [1, 2]. This technique is still in exploration and research stage. The research tasks mainly include imaging theory of digital lithography, design of digital lithography system, design of digital mask and resolution enhancement technique [3].

Peng Qinjun in Sichuan University in China, has presented the liquid crystal display (LCD), real-time grey-tone mask technique for fabrication of continuous microstructure [4], which combines the LCD system with the projection lithography system. Firstly, 3-D relief structure is converted to 2-D grey-tone pattern. Then the 2-D grey-tone pattern is decomposed into a series of binary patterns. By utilizing the LCD

panel to display a series of binary patterns, the continuous grey-tone record has been formed on the photoresist. After development and fixation, the desired relief structure can be obtained.

Based on the decomposition ideal converting grey-tone pattern to binary pattern, we present real-time mask-division technique based on DMD. In reference [5], the exposure experiment of division binary grating verifies the feasibility of mask--division technique. However, the theory of mask division has not been investigated deeply. To achieve the applicability of mask division technique, we simulate the exposure intensity distribution of division mask according to the theory of image formation in partially coherent light. And what is more, the theory of mask division is established. The appropriate exposure time calculated by mask-division theory results in better experimental results than that in reference [5].

2. Theory of real-time mask-division technique

2.1. Diffractive limitation

DMD-based digital lithography technique has caught wide attention recently [6–11]. DMD is one of the reflective SLMs, which has inherent advantages, such as high resolution, high brightness, high contrast and quick response. In order to obtain micron or even submicron feature size, the reduction-projection object lens must be added to the digital lithography system. The reduction-projection object lens corresponds to a low-pass filter, so the high-order diffraction cannot pass through it. Accordingly, the loss of high-frequency components representing the fine structure results in the decline of pattern quality in the image plane.

According to the diffraction grating theory, when the parallel beam is normally incident on the grating plane, the diffraction phenomenon will appear and the grating equation is satisfied:

$$d\sin\theta = k\lambda, \quad k = 0, \pm 1, \pm 2, \ldots \tag{1}$$

where d is the grating period, θ is the diffraction angle and λ is the incident wavelength. When d and λ are taken fixed value, the higher the diffraction order is, the bigger the diffraction angle is. We can observe that the distance between the zero order and other orders becomes bigger with the higher diffraction order. In order to change the number of receiving diffraction orders in a limited range, we can change the grating period. In Fig. 1, for the object lens with limited field angle, when the grating period becomes bigger, the receiving diffraction orders greatly increase.

According to Abbe imaging principle, coherent imaging includes two steps: firstly, the spatial spectrum distribution is formed by diffraction; secondly, the image similar to original object is formed by the superimposition of spectra in the image plane. In order to obtain the image identical with the original object, all spectra should be

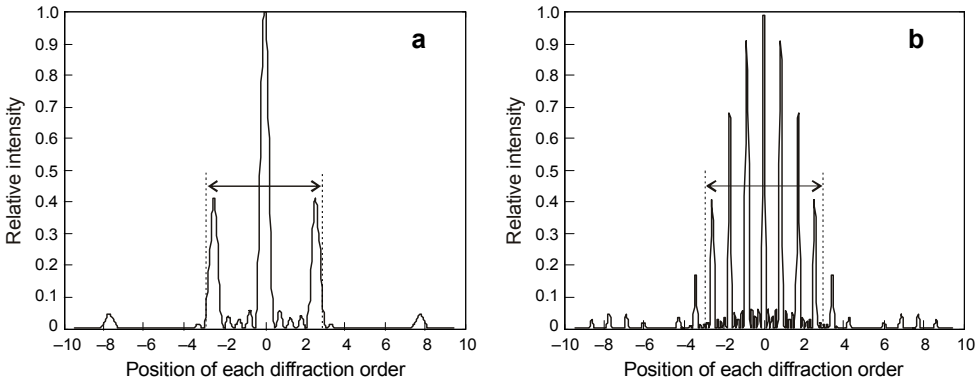

Fig. 1. Diffraction orders received by object lens with the change of grating period; $d = 10$ μm (**a**), $d = 30$ μm (**b**).

involved in imaging. The more the spectral components are involved in, the higher the similarity between object and image is. We demonstrate the influence of the spectra involved in imaging on the image structure. The transmission function of one-dimensional grating can be expressed by:

$$f(x) = \left[\text{rect}\left(\frac{x}{a}\right) \frac{1}{d} \text{comb}\left(\frac{x}{d}\right)\right] \text{rect}\left(\frac{x}{b}\right) \tag{2}$$

where a is the slit width, d is the grating period, and b is the grating width along the slit. The function of spectrum distribution can be given as:

$$F(f_x) = \frac{ab}{d} \sum_{-\infty}^{\infty} \text{sinc}\left(\frac{am}{d}\right) \text{sinc}\left[b\left(f_x - \frac{m}{d}\right)\right] \tag{3}$$

By applying inverse Fourier transformation to Eq. (3), we can get the image field distribution as follow:

$$g(x) = \frac{a}{d} \text{rect}\left(\frac{x}{b}\right)\left[1 + 2 \sum_{m=1}^{\infty} \text{sinc}\left(\frac{ma}{d}\right) \cos\left(\frac{2\pi mx}{d}\right)\right] \tag{4}$$

Similarity between $g(x)$ and $f(x)$ represents similarity between original object and its image. Figure 2**a** shows the effect when the diffraction orders from 0 to 6 are involved in imaging. Figure 2**b** shows the effect when the diffraction orders from 0 to 15 are involved in imaging. It is obvious that the image field distributions in Fig. 2**b**

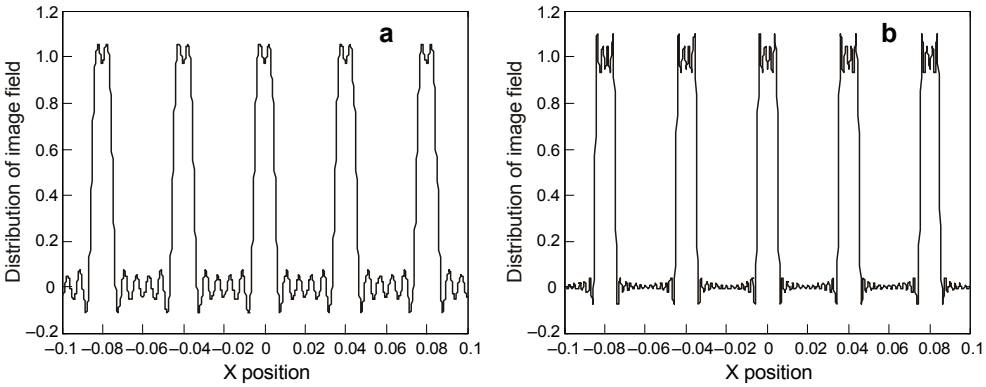

Fig. 2. Image field distribution with different orders involved in imaging; $m = 6$ (**a**), $m = 15$ (**b**).

are more similar to the original object. Due to the finite aperture of projection object lens, we have to lower the spatial frequency of the mask to increase the imaging spectrum.

2.2. Theory of mask division

Real-time mask-division technique consists in dividing a piece of a high-frequency mask into a series of low-frequency masks by fixed or variable low-frequency period sampling. Hence, each period of a low-frequency mask includes several periods of the undivided high-frequency mask. Using real-time mask technique, these low--frequency masks are exposed in sequence. The superimposed lithography effect of these low-frequency masks is the same as that of the original high-frequency mask. So the original high-frequency mask can be recovered by these low-frequency masks. For a piece of the high-frequency binary grating mask, the diffraction angle corresponding to high-order diffraction is big. Without mask division, the loss of middle and high components is serious, which will result in the fuzzy edge of lithography pattern.

We explain the theory by using a high-frequency grating. When dividing a piece of high-frequency grating mask into N pieces of low-frequency grating mask, these low-frequency grating masks are displayed on DMD one by one. After being imaged by object lens, the intensity distribution of each binary grating mask on a photoresist is supposed to be I_n ($n = 1, \ldots, N$), the total exposure on the photoresist can be expressed by

$$E = \sum_{n=1}^{N} I_n t_n \tag{5}$$

where t_n represents the displaying time of each frame, namely the exposure time. Considering the periodic structure of the grating, we believe that each frame has

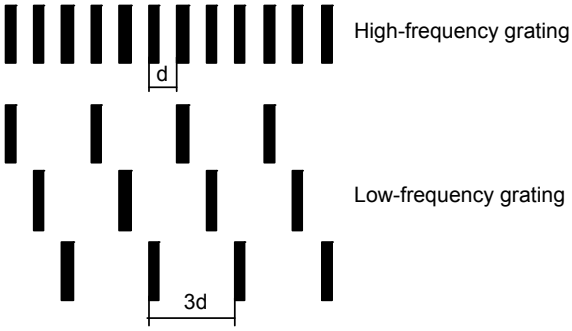

Fig. 3. Triple-division grating.

the same exposure time and we do not take into account the nonlinear effect of the photoresist. The total exposure time is defined as t according to the required exposure of the original high-frequency grating

$$t_n = \frac{t}{N} \tag{6}$$

Two aspects should be considered when choosing N: one is the fabrication quality and the other is the fabrication efficiency. When N is great, DMD displays more frames. So the displaying time is very long and the fabrication efficiency is low. When N is small, the mask division is ineffective. Supposing that the period of high-frequency mask is d and the period of low-frequency mask after division is d_n (n = 1, ..., N), the relation between d and d_n can be given as

$$d_n = \frac{d}{N} \tag{7}$$

According to above theory, we design the program of real-time mask division. Figure 3 shows the principle of a triple-division grating. The division masks are displayed on DMD in turn. The position of each division mask is strictly controlled by computer program, so the alignment error is avoided.

3. Simulation results of real-time mask division

Taking the triple-division grating in Fig. 3 as an example, we respectively simulate the intensity distribution of high-frequency grating and low-frequency grating after being imaged on the photoresist. During simulation, the linear photosensitization of the photoresist is supposed. For division mask, calculation of the total superimposed exposure includes several steps: firstly calculating the intensity distribution of each division mask after being imaged on the photoresist, then calculating the exposure distribution of each division mask, finally summing the exposure of all division masks. When choosing the intensity distribution model in the image plane, the type of light source in lithography system should be considered. The mercury lamp, which has

poor coherence, is usually adopted as a light source in UV lithography system. When the light propagates to the mask plane, it becomes partially coherent light according to the Van Cittert–Zernike theorem. Hence, the theory of partially coherent imaging is chosen for simulation. According to the concept of equivalent light source, the intensity distribution in the image plane can be expressed as:

$$I(x_i, y_i) = \iint_{\sigma} I_{\text{eff}}(x_s - f_x, y_s - f_y) \left| F^{-1}\left\{ F^{-1}\left\{ \text{MASK}(x, y) \right\} H(x_s - f_x, y_s - f_y) \right\} \right|^2 \mathrm{d}x_s \mathrm{d}y_s \tag{8}$$

where $I_{\text{eff}}(x_s, y_s)$ represents the intensity distribution of an effective source and $H(x_s - f_x, y_s - f_y)$ represents the pupil function. $F^{-1}\{\text{MASK}(x, y)\}$ represents the object spectrum, namely the Fourier transform of mask function. In simulation, the partially coherent factor σ, the numerical aperture of object lens NA and the wavelength λ are respectively taken 0.5, 0.3 and 365 nm. Figure 4 shows the exposure distribution of the original high-frequency grating. Figure 5 shows the exposure distribution of single low-frequency division grating. Figure 6 shows the superimposed exposure distribution of three pieces of low-frequency division gratings. Simulation results indicate that the superimposed lithography effect of division masks is the same as that of the original

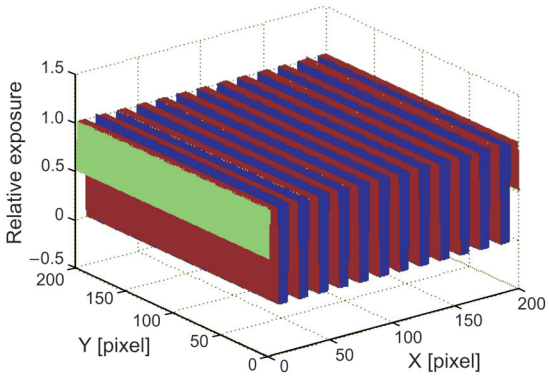

Fig. 4. Exposure dose distribution of high--frequency grating mask.

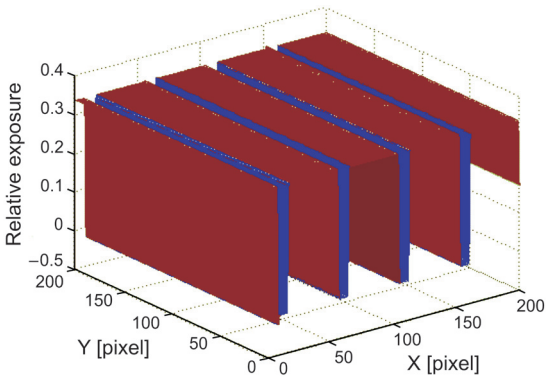

Fig. 5. Exposure dose distribution of one piece of division-grating mask.

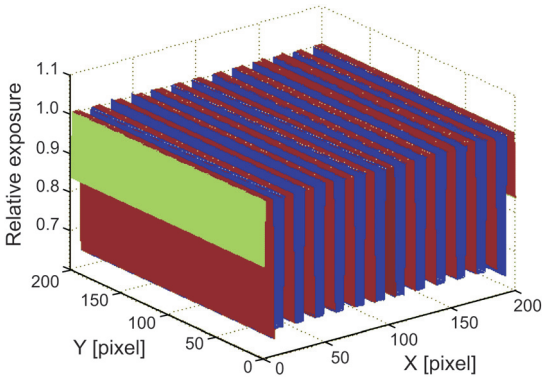

Fig. 6. Superimposed exposure dose distribution of three pieces of division grating--mask.

high-frequency mask. Due to many influencing factors in lithography, some differences between the actual exposure and the ideal exposure exist.

4. Experiments and analysis

4.1. Theoretical analysis

The DMD-based digital lithography system has been set up. Figure 7 shows the system schematic diagram. The 200 W mercury lamp is used as a light source and the dominant wavelength is 365 nm. Fly eyes are used to obtain even illumination. The positive photoresist of RZJ304 is adopted as recording material and the photosensitive range is from 350 nm to 450 nm.

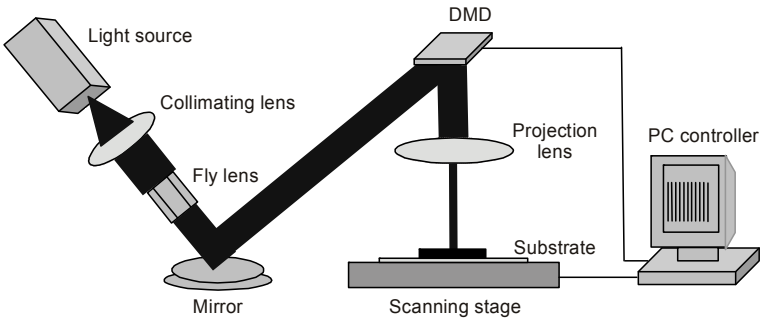

Fig. 7. Schematic of the DMD-based digital lithography system.

The resolution of reduction-projection object lens is 1 μm and NA is 0.3. We find that the exposure error is great due to the serious loss of high-frequency components caused by diffractive limitation during imaging. Supposing that the field angle is 45°, the highest order that the object lens receives can be obtained by

$$k = \frac{d \sin \theta}{\lambda} \tag{9}$$

When the grating period is 2 μm and the duty ratio is 1:2, the object lens can only receive three orders including 0 and ±1. The diffraction efficiency of even order is 0 and the diffraction efficiency of the first order is only 40.5%. For binary grating, the diffraction efficiency of each order is given by

$$\eta_m = \frac{4\sin^2(n\pi M)}{(n\pi)^2} \qquad (m = 1, 2, 3, ...) \tag{10}$$

where M represents the duty ratio. According to Eq. (10), the diffraction orders of 0 and ±1 occupy 81% of the diffraction efficiency. The lost middle and high orders (above ±1) account for 19%. By triple division, the duty ratio changes to 1:6 and the grating period turns into 6 μm. According to Eq. (9), the object lens can receive thirteen orders from 0 to ±6. Here the diffraction orders of 0 and ±1 occupy 36.5% of the diffraction efficiency. The lost middle and high orders (above ±6) account for 11.6%. The above analysis indicates that the mask-division technique can greatly increase the number of diffraction orders received by object lens and effectively decrease the loss of middle and high frequency components with edge information.

Whether a mask needs division depends on the feature size of a mask. It is unnecessary for the mask with a large feature size because the object lens can receive more diffraction orders. The division mainly aims at the mask with a small feature size (≤ 4 μm).

4.2. Experimental results

Based on the feature of DMD-based digital lithography system and mask-division technique, we choose the grating with a feature size of 4 μm for division experiments. Figure 8**a** shows the lithography pattern with the original mask after single exposure. Figure 8**b** is the reconstruction pattern for Fig. 8**a**. Figure 9**a** shows the lithography

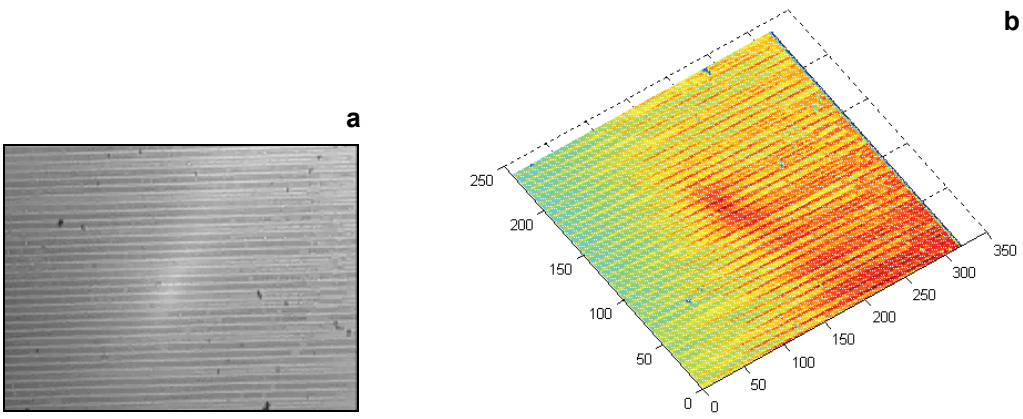

Fig. 8. Experimental results of 4 μm grating. Relief structure on photoresist after single exposure (**a**); reconstruction pattern (**b**).

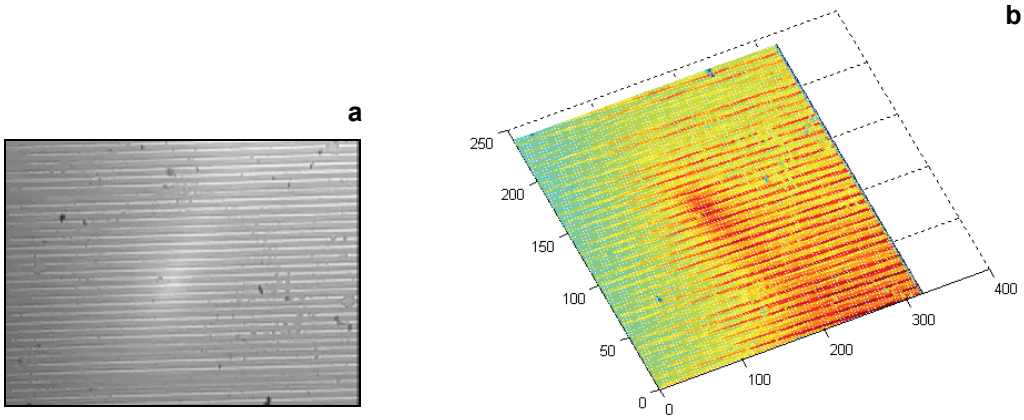

Fig. 9. Experimental results of 4 μm grating by mask-division method. Relief structure on photoresist after superimposed exposure (**a**); reconstruction pattern (**b**).

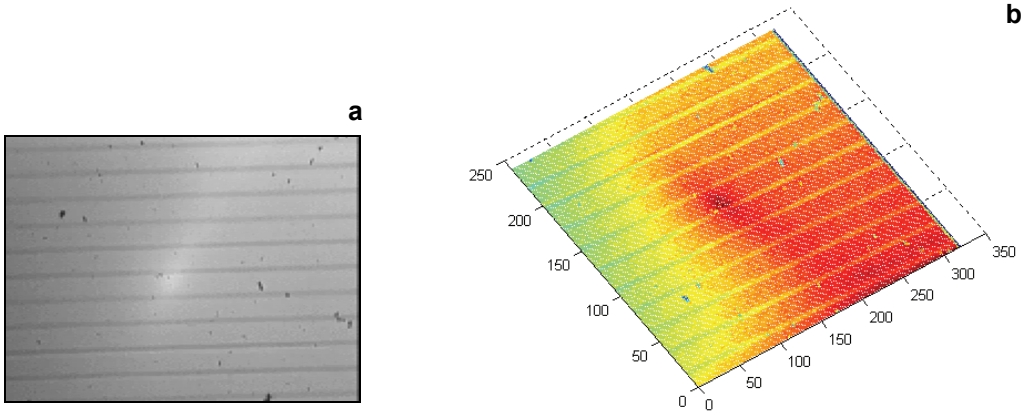

Fig. 10. Experimental results of one piece of division-grating mask. Relief structure of one piece of division-grating mask (**a**); reconstruction pattern (**b**).

pattern with three pieces of division masks after superimposed exposure. Figure 9**b** is the reconstruction pattern for Fig. 9**a**. Figure 10**a** shows the lithography pattern with single division mask. Figure 10**b** is the reconstruction pattern for Fig. 10**a**. Comparing Fig. 8 with Fig. 9, we find that the contrast of grating lines is better and the edge of lines is clearer in Fig. 9.

5. Conclusions

The real-time mask-division technique based on DMD digital lithography for improving the lithography quality has been described. It is based on the decomposition idea of binary pattern and diffraction grating theory. The real-time mask-division technique is to divide a piece of high-frequency mask into a series of low-frequency

masks. These low-frequency masks are displayed on DMD one by one. The superimposed lithography effect with these low-frequency masks can take the place of that with the original high-frequency mask. After development and fixation, the desired relief structure can be formed on the photoresist. Experimental results prove that the edge sharpness and lithography quality can be effectively improved when fabricating the small feature size. The technique is effective on fabrication of grating and Fresnel lens with small feature size. It is useful for high-frequency grey-tone digital mask as well. The further research has to show how to decompose high-frequency grey-tone mask into low-frequency binary mask.

Acknowledgements – This work was supported by Key Laboratory of Nondestructive Test (Chinese Ministry of Education) in Nanchang HangKong University. The authors appreciate the support of the National Natural Science Foundation of China (No.60777046) and the funds of Aerial University (No.EC200808184).

References

[1] TAKAHASHI K., SETOYAMA J., *An UV-exposure system using DMD*, Transactions of the Institute of Electronics, Information and Communication Engineers **J82-C-2**(3), 1999, pp. 92–94 (in Japanese).

[2] KIN FOONG CHAN, ZHIQIANG FENG, REN YANG, AKIHITO ISHIKAWA, AND WENHUI MEI, *High-resolution maskless lithography*, Journal of Microlithography, Microfabrication, and Microsystems **2**(4), 2003, pp. 331–339.

[3] LIANG YIYONG, YANG GUOGUANG, *Linewidth control by overexposure in laser lithography*, Optica Applicata **38**(2), 2008, pp. 399–404.

[4] PENG QINJUN, GUO YONGKANG, ZENG YANGSU, LIU SHIJIE, CHEN BO, XIAO XIAO, *Real-time grey-tone mask technique for fabrication of microlens array*, Chinese Journal of Lasers **30**(10), 2003, pp. 893–896.

[5] SHEN TINGZHENG, LV HAIBAO, GAO YIQING, QI XINMIN, LUO NINGNING, *Research of mask division for improving the edge sharpness of photolithography*, Acta Optica Sinica **25**(4), 2005, pp. 533–537.

[6] YIQING GAO, TINGZHENG SHEN, JINSONG CHEN, NINGNING LUO, XINMIN QI, QI JIN, *Research on high-quality projecting reduction lithography system based on digital mask technique*, Optik **116**(7), 2005, pp. 303–310.

[7] XIAOWEI GUO, JINGLEI DU, YONGKANG GUO, CHUNLEI DU, ZHENG CUI, JUN YAO, *Simulation of DOE fabrication using DMD-based grey-tone lithography*, Microelectronic Engineering **83**(4–9), 2006, pp. 1012–1016.

[8] MANSEUNG SEO, HAERYUNG KIM, *Lithography upon micromirrors*, CAD Computer Aided Design **39**(3), 2007, pp. 202–217.

[9] BEASLEY B.D., BENDER M.W., CROSBY J., MESSER T., SAYLOR D.A., *Advancements in the micromirror array projector technology*, Proceedings of SPIE **5092**, 2003, pp. 71–82.

[10] KIN FOONG CHAN, ZHIQIANG FENG, REN YANG, WENHUI MEI, *High-resolution maskless lithography by the integration of micro-optics and point array technique*, Proceedings of SPIE **4985**, 2003, pp. 37–43.

[11] ERDMANN L.H., DEPARNAY A., WIRTH F., BRUNNER R., *MEMS-based lithography for the fabrication of micro-optical components*, Proceedings of SPIE **5347**, 2004, pp. 79–84.

Received February 8, 2009
in revised form June 23, 2009